A novel second-order sliding mode control of hybrid fuel cell/super capacitors power system considering the degradation of the fuel cell

Yue Zhou, Hussein Obeid, Salah Laghrouche, Mickaël Hilairet, Abdesslem Djerdir

A novel second-order sliding mode control of hybrid fuel cell/super capacitors power system considering the degradation of the fuel cell

Y.Zhou[a], H.Obeid[b], S.Laghrouche[a], M.Hilairet[a], A.Djerdir[a]

[a]*FEMTO-ST Institute, FCLAB, Université Bourgogne Franche-Comté,UTBM, CNRS, Rue Ernest Thierry Mieg, F-90000 Belfort, France*
[b]*NORMANDIE UNIV, UNICAEN, LUSAC, 14000 Caen, France*

Abstract

This paper aims to design a novel control strategy of a single converter hybrid power system including a Proton Exchange Membrane Fuel Cell (PEMFC) and super capacitors for electric vehicle applications. The control objective to be addressed in such systems is to smooth the current of PEMFC considering the transient power and sinusoidal disturbance from the load. Moreover, in real-time applications, it is required to ensure the operation by taking into account the component constraints and the degradation of PEMFC. To achieve these goals, a robust nonlinear cascaded voltage control loop is developed in this paper. For the inner voltage loop, a second order twisting controller with dynamic saturation scheme is adopted to ensure the convergence of the DC bus voltage to its reference value as well as to attenuate the oscillations on PEMFC current. For the outer voltage loop, a Proportional Integral controller (PI) with anti-windup scheme is utilized to control the super capacitors voltage at its desired value. Furthermore, in order to consider the degradation of PEMFC in the controlled system, an estimation of the degradation model parameters has been provided by Cubature Kalman filter. Comparative Hardware-in-the-loop (HIL) tests between the proposed control strategy and the traditional two PI controllers strategy for the hybrid power system is performed. The results of HIL tests verified the effectiveness of the proposed nonlinear control strategy.

Keywords: Hybrid electric vehicle, proton exchange membrane fuel cell degradation, second order twisting controller, super capacitors, Hardware-in-the-loop test bench

1. Introduction

In the last few years, with the increasing pressure of energy crisis and environmental protection, fuel cell technologies have received wide attention and application from all over the world [1–3]. Among the current fuel cell technologies, the Proton Exchange Membrane Fuel Cell (PEMFC) is regarded as the most hopeful choice for vehicle and portable applications due to the numerous advantages of high energy efficiency, low operating temperature, no corrosive fluid hazards, and small size [4, 5]. In spite of these good points, there are still some deficiencies caused by the inherent characteristics of PEMFC [6, 7]. One of the main deficiencies of PEMFC is slow dynamic due to the hydrogen delivery system. Thus, when facing a step demand of load or the load with sudden perturbations, PEMFC will occur fuel starvation phenomena, which will decrease the lifespan of membranes and influence the performance of PEMFC [8]. For these transient loads mentioned above, a fast dynamic auxiliary power source is necessary to be utilized. Compared with battery, super capacitors (SCs) are considered as a better choice as auxiliary source in terms of high power density, good energy effectiveness and high lifespan (superior than one million cycles). Furthermore, SCs are able to work at even low temperature, such as -20 °C [9]. Therefore, SCs are chosen as auxiliary power source while PEMFC is considered as the main power source in this paper.

The architectures for hybrid fuel cell/SCs power system can be divided into three categories: parallel, series and cascaded. Due to the benefits of high reliability and low component stresses, parallel architecture is regarded as the most suitable architecture [10, 11]. For parallel architectures of hybrid fuel cell/SCs power system, there are three types of topologies [9, 12]. The first type is fully-active topology, which consists of two DC/DC converters and each converter is linked to a power source. The second type is passive topology, in which no DC/DC converter is adopted. The main advantage of the first type topology is flexible control performance while the disadvantage is higher costs for expenses. For the second type topology, it costs less but it has the lower controllability. Hence, taking into account a promising balance between the economy and control performance, the third type topology, namely semi-active topology on the basis of a single converter is utilized in this study.

Currently, there are various control strategies for hybrid multi-source power system studied by other researchers, such as proportional integral (PI) controller and passivity-based controller [13, 14]. However, among these previous researches on control strategies, the solution of suppressing disturbance for a hybrid fuel cell/SCs power system with only one converter is not considered. Moreover, these mentioned control methods have not taken into account the degradation phenomenon of the hybrid power system. When the hybrid system operates, both the PEMFC and the super capacitors will experience degradation in performance. In the long-term operation of the PEMFC, the electrical resistance, exchange current, and limiting current of the PEMFC will change [15]. Compared with PEMFC, the service life for the super capacitors is longer to a large extent. Due to this fact, degradation phenomenon of SCs is ignored in this study [16]. Therefore, the degradation phenomenon of the PEMFC as well as the external disturbance should be taken into account in the design of the control strategy to effectively improve the dynamic response of the hybrid power system.

Sliding mode control approach is one of the most efficient methods for controlling systems with parametric uncertainties and external disturbances [17–21]. Among the sliding mode controllers, the twisting controller is the conventional second order sliding mode control that is applied for perturbed systems with relative degree two affected by bounded disturbance [22, 23]. However, this controller provides a discontinuous control signal. In order to obtain a continuous control signal and still have finite time convergence, the idea of relative degree extension can be used [24]. This idea consists in considering the extra equation $\dot{u} = v$, where u is a real control input and v is a virtual higher order sliding mode discontinuous control input.

The aim of this paper is to develop a robust control strategy for the hybrid power system with a single converter considering the degradation phenomenon of PEMFC and the external disturbance. This control strategy should reject the sudden disturbance and decrease the oscillations on fuel cell current, i.e. provide a smooth behavior of the fuel cell current. To that purpose, and inspired by the idea of relative degree extension, our strategy proposes the usage of twisting controller as virtual control input to regulate the DC bus voltage to its reference value. Hence, this strategy ensures the finite time convergence of the DC bus voltage to its reference value while compensating the parametric uncertainty and the external disturbance. Moreover, it provides a continuous control signal which leads to smooth the fuel cell current and increase the lifespan of PEMFC. The main

contributions of this work are the following:

1. The degradation estimation of PEMFC is researched by the method of Cubature Kalman Filter (CKF). The CKF accurately estimates the degradation state and degradation rate for PEMFC. The estimated degradation of PEMFC is applied to the control of the hybrid power system.

2. A robust cascaded voltage control loop is developed on the basis of twisting controller and PI controller for the single converter hybrid power system integrating the degradation of PEMFC. For protection purpose, the constraints of fuel cell and super capacitors are taken into account in the proposed control scheme.

3. The effectiveness of the proposed control strategy is validated by HIL test experiment. Indeed, the HIL test results show that the proposed control method has better performance than the traditional two PI controllers in view of disturbance suppression in the hybrid fuel cell/SCs power system.

The organization of this paper is as follows: In section 2, the description of the hybrid fuel cell/SCs power system based on a single converter is detailed. In section 3, the degradation model of PEMFC based on the PEMFC degradation experiment is firstly given. Then, the PEMFC degradation estimation is made by CKF method. In section 4, the proposed control strategy with limitation constraints for this hybrid power system is described. In section 5, the HIL test results are illustrated to validate the effectiveness of the proposed control strategy. Finally, in section 6, the main conclusions are presented.

2. Hybrid fuel cell/SCs power system

2.1. Configuration of hybrid fuel cell/SCs power system

The topology of the hybrid fuel cell/SCs power system is presented in Fig.1. The configuration characteristic is a parallel architecture on the basis of a single DC/DC converter, which has taken into account the balance between the economy and control performance compared with other configurations.

As shown in Fig.1, in this hybrid power system, the fuel cell system which provides the main power is linked to the DC bus directly and the SCs pack which supplies the transient power is linked to the DC bus by a bidirectional DC/DC converter.

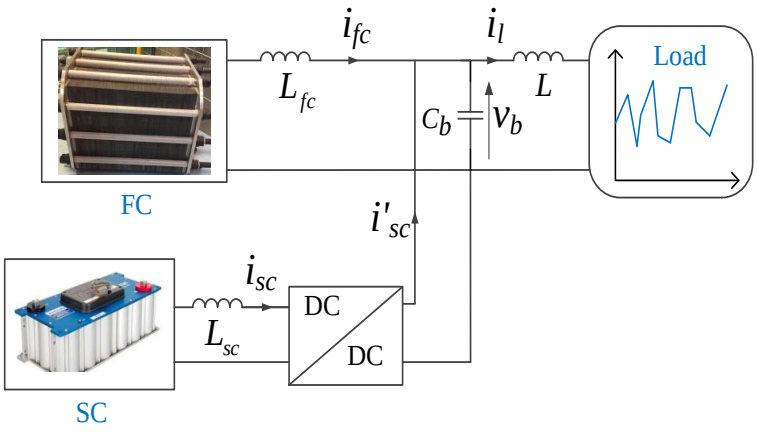

Figure 1: Hybrid system topology

2.2. Model of PEMFC

PEMFC is a kind of fuel cell that uses hydrogen fuel to react with air to generate electricity and heat. PEMFC is mainly developed for transport applications [25]. Usually, a PEMFC stack is composed of multiple cells. Each cell includes proton exchange membrane, electrode, catalyst, gas diffusion layer, and bipolar plate [26].

The output characteristics of PEMFC can usually be represented by the polarization curve, as shown in Fig.2, according to [27]. When the output current is small, the output voltage of PEMFC is mainly affected by the activation polarization [28]. The speed of the activation reaction can be expressed by the exchange current of PEMFC. With the increase of the exchange current, the electrode surface reaction will be more and more active and the activation over potential will grow smaller. When the output current is large, the output voltage of PEMFC is mainly affected by concentration polarization. The loss of voltage is mainly determined by the concentration of reactants and products [29]. The limiting current of PEMFC is usually used to indicate the intensity of the concentration polarization. The larger the limiting current is, the smaller the loss of voltage will be. Ohmic polarization is caused by the resistance of electrons through the electrode material and the connecting parts, and the protons pass through the membrane. The electrical resistance is usually adopted to indicate the intensity of the concentration polarization. Therefore, the output voltage of PEMFC can be expressed as (1) [15].

$$V_{fc} = E_r - ATln(\frac{i_{fc}}{i_o}) - i_{fc}R_{fc} - BTln(\frac{i_{lim}}{i_{lim} - i_{fc}}), \quad (1)$$

where V_{fc} is the output voltage of PEMFC, i_{fc} is the current of PEMFC, E_r is the theoretical potential of PEMFC, i_o is the exchange current of PEMFC, i_{lim} is the limiting current of PEMFC, R_{fc} is the electrical resistance of PEMFC, A is the Tafel slope, B is the mass transfer constant, and T is the operating temperature of PEMFC.

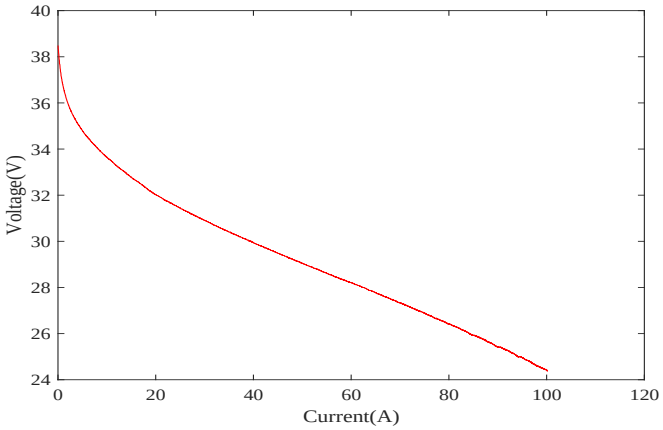

Figure 2: The polarization curve of PEMFC

2.3. Model of super capacitors

The SCs pack as a voltage source type electrical energy storage element has the advantages of high power density, long lifespan, short charging and discharging time, high reliability and so on. There are a variety of models for developing SCs pack in the existing literature [30]. In this paper, SCs pack is modeled by a voltage source connected to a pure inductor.

3. PEMFC degradation

3.1. PEMFC degradation experiment

The PEMFC degradation experiment is performed in the FCLAB [27], as shown in Fig.3. The membrane adopts Nafion membrane, and the electrode adopts the platinum nanoparticle catalyst. The PEMFC is operated under constant load current for 1000 h. The PEMFC operating conditions are shown in Table 1.

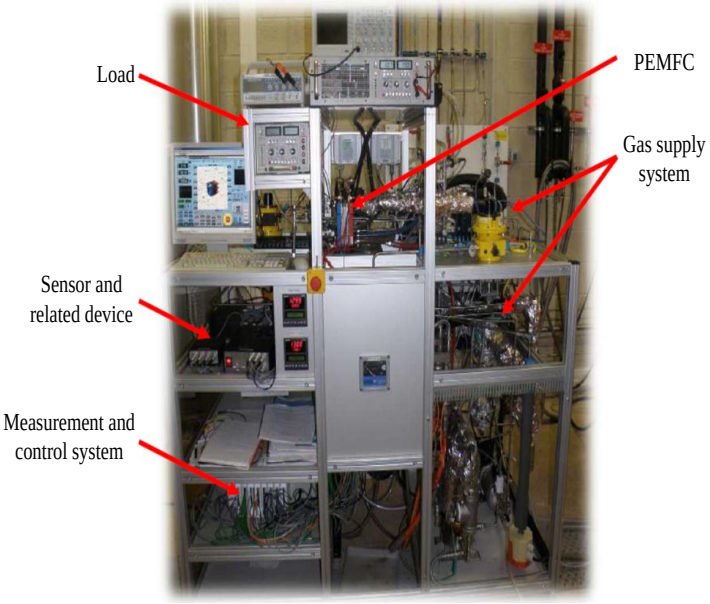

Figure 3: The PEMFC degradation testing platform

Table 1: The operating parameters of PEMFC

Parameter	Value
Number for cells	5
Active area	100 cm^2
Membrane thickness	25 μm
Platinum catalyst	0.2 mg/cm^2
GDL thickness	415 μm
Load current	70 A
Hydrogen pressure	1.3 bar
Temperature	54 °C
Relative humidity	52%

3.2. PEMFC degradation model

According to the literatures [31–33], resistance and limiting current vary greatly during the PEMFC degradation. The relationship between resistance and limiting current over time can be expressed as the following equations.

$$R_{fc}(t) = R_{fc}(0)(1 + \alpha(t)), \tag{2}$$

$$i_{lim}(t) = i_{lim}(0)(1 - \alpha(t)), \tag{3}$$

$$\alpha(t) = \beta t, \tag{4}$$

where α represents the state of health (the indicator of degradation of PEMFC), and β represents the speed of degradation.

3.3. Degradation estimation based on Cubature Kalman Filter

The nonlinear system is represented by the following equations.

$$x_{k+1} = f(x_k, u_k) + w_k, \tag{5}$$

$$y_{k+1} = h(x_{k+1}, u_k) + v_k, \tag{6}$$

where x=$[\alpha; \beta]$ is the system state, y= $[V_{fc}]$ is the output state of system, u_k is the input of system, f is the state transfer function from x_k to x_{k+1}, h represents the system measurement function, w_k and v_k represent the system process noise and system measurement noise respectively. The w_k and v_k are considered as the Gaussian noises with zero mean and covariance Q and R.

The CKF based on the spherical-radial cubature rule produces a set of cubature points to estimate the state of a nonlinear system [34, 35]. Since the cubature rule does not require derivatives, the CKF has less computational effort [36]. Compared with conventional nonlinear filters, CKF has higher filtering accuracy [34]. The basic process of CKF state estimation is shown below:

1). Initialization: initialize state and covariance

$$\hat{x}_0 = E[x_0],\ P_0 = Var[x_0]. \tag{7}$$

2). Calculate cubature points

$$P_k = S_k S_k^T, \tag{8}$$

$$x_k^i = S_k\gamma_i + \hat{x}_k,\ i = 1, 2, ..., 2n, \tag{9}$$

where n is the dimension of state variables, γ_i is a set of cubature points.

$$\gamma_i = \begin{cases} \sqrt{n}E_i,\ i = 1, 2, ..., n \\ -\sqrt{n}E_i,\ i = n+1, n+2, ..., 2n \end{cases} \tag{10}$$

where E_i is the unit matrix.

3). Cubature points propagation

$$x_{k+1|k}^i = f(x_k^i, u_k). \tag{11}$$

4). State prediction

$$\hat{x}_{k+1|k} = \frac{1}{2n}\sum_{i=1}^{2n} x_{k+1|k}^i, \tag{12}$$

$$\bar{p}_k = \frac{1}{2n}\sum_{i=1}^{2n} x_{k+1|k}^i (x_{k+1|k}^i)^T - \hat{x}_{k+1|k}(\hat{x}_{k+1|k})^T + Q. \tag{13}$$

5). Cubature points calculation

$$\bar{p}_k = S_{k+1|k}S_{k+1|k}^T, \tag{14}$$

$$X_{k+1|k}^i = S_{k+1|k}\gamma_i + \hat{x}_{k+1|k}. \tag{15}$$

6). Cubature points propagation

$$y_{k+1}^i = h(X_{k+1|k}^i, u_k). \tag{16}$$

7). Measurement update

$$\hat{y}_{k+1} = \frac{1}{2n}\sum_{i=1}^{2n} y_{k+1}^i, \tag{17}$$

$$p_{yy} = \frac{1}{2n}\sum_{i=1}^{2n} y_{k+1}^i (y_{k+1}^i)^T - \hat{y}_{k+1}\hat{y}_{k+1}^T + R, \tag{18}$$

$$p_{xy} = \frac{1}{2n}\sum_{i=1}^{2n} X_{k+1|k}^i (y_{k+1}^i)^T - \hat{x}_{k+1|k}\hat{y}_{k+1}^T. \tag{19}$$

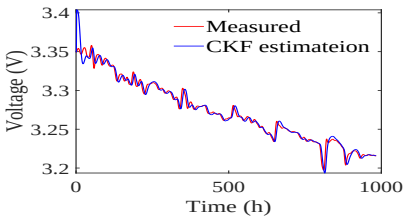

(a) PEMFC voltage estimation

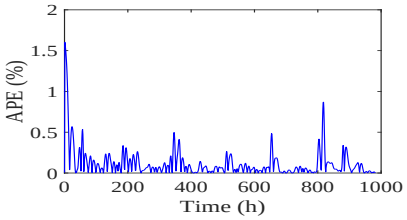

(b) The APE of PEMFC voltage estimation

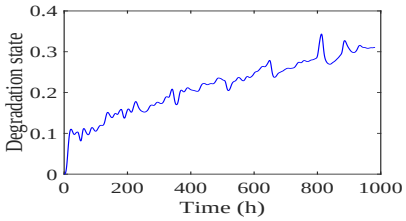

(c) The estimation of PEMFC degradation state (α)

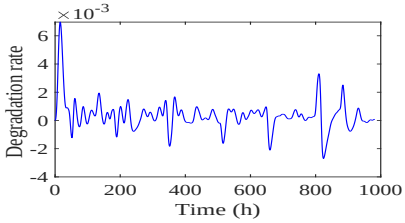

(d) The estimation of PEMFC degradation rate (β)

Figure 4: Degradation estimation based on CKF

8). State and covariance update: Estimate the Kalman gain K, state $\hat{x}_{k+1}$ *and covariance* P_{k+1}

$$K = p_{xy}p_{yy}^{-1}, \tag{20}$$

$$\hat{x}_{k+1} = \hat{x}_{k+1|k} + K(y_{k+1} - \hat{y}_{k+1}), \tag{21}$$

$$P_{k+1} = \bar{p}_k - Kp_{yy}K^T. \tag{22}$$

The degradation state α and degradation rate β of the PEMFC degradation model are estimated by the CKF. As shown in Fig.4(a), the estimated voltage is close to the measured voltage of PEMFC. As shown in Fig.4(b), the maximum Absolute Percentage Error (APE) between the measurement voltage and CKF estimated voltage is less than 1.8%. The mean APE between the measurement voltage and CKF estimated voltage is about 0.11%. As shown in Fig.4(c), with the operation of the PEMFC, the degradation state of the PEMFC increases. As shown in Fig.4(d), the mean degradation rate is about 0.0003. The estimated degradation state and degradation rate are applied to design the control systems.

4. Design of control strategy

4.1. Control Structure

The control structure of hybrid fuel cell/SCs power system is illustrated in Fig.5. The proposed control strategy is on the basis of a cascaded control loop.

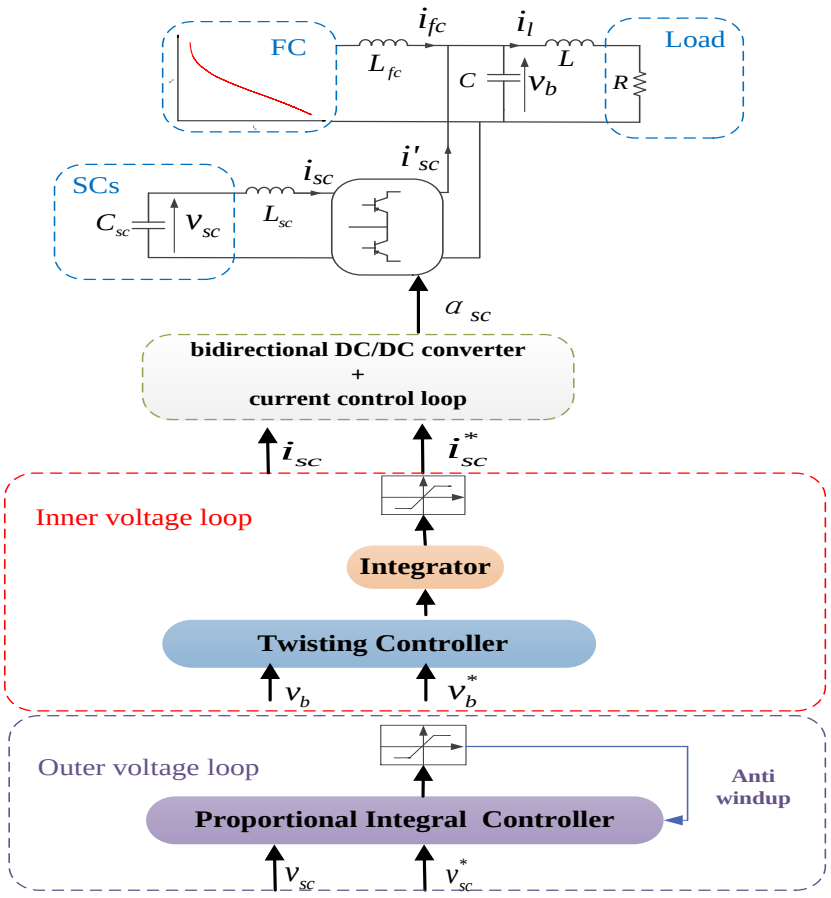

Figure 5: Control structure diagram

As shown in Fig.5, the SCs reference current i^*_{sc} is transmitted by the DC bus and the SCs current i_{sc} is regulated by the bidirectional DC/DC controller with its own current controller. In the inner voltage loop, a twisting controller with an integrator and saturation functions is proposed in order to guarantee the convergence of the voltage of the DC bus at its reference value,

while compensating the external perturbation; in the outer voltage loop, a PI controller with an anti-windup scheme is utilized in order to regulate the voltage of SCs at its nominal condition.

The complete hybrid fuel cell/ SCs system can be expressed as following equations:

$$\frac{d}{dt}v_b(t) = \frac{i_{fc}(t) + (1 - a_{sc}(t))i_{sc}(t) - i_l(t)}{C}, \tag{23}$$

$$\frac{d}{dt}v_{sc}(t) = -\frac{i_{sc}(t)}{C_{sc}}, \tag{24}$$

$$\frac{d}{dt}i_{sc}(t) = \frac{v_{sc}(t) - v_b(t)(1 - a_{sc}(t))}{L_{sc}}, \tag{25}$$

$$i_{fc}(t) = \frac{V_{fc}(t) - v_b(t)}{R_{fc}(t)}, \tag{26}$$

where a_{sc} is the duty cycle of the bidirectional DC/DC converter, $i_{fc}(t)$ is the current of fuel cell, $i_{sc}(t)$ is the current of SCs, $i_l(t)$ is the current of the load, $v_{sc}(t)$ is the voltage of SCs and $v_b(t)$ is the DC bus voltage, with state space $x(t) = [v_b; v_{sc}; i_{sc}]^T$, control input $u(t) = a_{sc}$, measurements $y(t) = [i_{fc}; i_{sc}; i_l; v_b; v_{sc}]$.

Considering the degradation of fuel cell, according to the degradation model detailed in section 3, $V_{fc}(t)$ in equation (26) can be rewritten as following equation:

$$V_{fc}(t) = E_r - ATln(\frac{i_{fc}(t)}{i_o}) - i_{fc}(t)R_{fc}(0)(1+\alpha(t)) - BTln(\frac{i_{lim}(0)(1-\alpha(t))}{i_{lim}(0)(1-\alpha(t)) - i_{fc(t)}}), \tag{27}$$

where the degradation state $\alpha(t)$ can be expressed as βt, in which β represents the degradation speed of fuel cell.

In order to design the twisting controller for the inner voltage loop, the bandwidth of the bidirectional DC/DC converter current control loop is assumed as decoupled to the inner voltage loop. Thus, it can be deduced that the controller current of SCs is equal to the reference current of SCs which is calculated from the inner voltage loop on the basis of twisting controller. Under the previous assumption, the following equation can be obtained, as shown in equation (28).

$$L_{sc}\frac{d}{dt}i_{sc}(t) = 0. \tag{28}$$

Substitute equation (28) into the equation (25), then:

$$v_{sc}(t) - v_b(t)(1 - a_{sc}(t)) = 0. \tag{29}$$

The above equation can be represented as follows.

$$a_{sc}(t) = 1 - \frac{v_{sc}(t)}{v_b(t)}. \tag{30}$$

Thus, the expression of the DC bus voltage is shown as equation (31) and (32), in which $i'_{sc}(t)$ is the new input variable in this reduced system currently.

$$C\frac{d}{dt}v_b(t) = i_{fc}(t) + i'_{sc}(t) - i_l(t), \tag{31}$$

with

$$i'_{sc}(t) = \frac{v_{sc}(t)}{v_b(t)}i_{sc}(t). \tag{32}$$

4.2. Inner voltage controller

The main objective of the inner voltage loop is to regulate the DC bus voltage to its reference value while rejecting the external disturbance and taking into account the degradation of the PEMFC.

In this work, the inner voltage controller utilizes the idea of relative degree extension where the virtual control input is chosen as twisting controller. This controller is well-known by its robustness in presence of system uncertainty and unexpected fluctuations [37]. Indeed, it provides a discontinuous control signal and ensures the finite time convergence of the state variable and its derivative to the origin for systems with relative degree two [38, 39]. It has been widely used in different areas, such as power systems, power converters, electrical drives and robot manipulators [40].

In the considered hybrid power system, the dynamics of the DC bus voltage can be expressed as a first order disturbed system as shown in equation (31). Due to that and in order to implement the twisting controller algorithm, the idea of relative degree extension has been used. The application of this idea will be described now in detail.

Let us first define $\phi(t) = i_{fc}(t)+i'_{sc}(t)-i_l(t)$ as a new auxiliary state, then the dynamics of the DC bus voltage given by equation (31) can be expressed as

$$\begin{aligned} C\frac{d}{dt}v_b(t) &= \phi(t), \\ \dot{\phi}(t) &= v(t), \end{aligned} \tag{33}$$

where $v(t)$ is the new virtual control input to be designed.

Now, let us define the sliding variable $s_{vb}(t)$ and its derivative $s_\phi(t)$ for the DC bus voltage as follows

$$\begin{aligned} s_{vb}(t) =& C(v_b(t) - v_b^*(t)), \\ s_\phi(t) =& \phi(t) - C\dot{v}_b^*(t), \end{aligned} \tag{34}$$

where $v_b^*(t)$ is the reference DC bus voltage obtained from the outer voltage loop and that will be designed later. Taking the first derivative of $s_{vb}(t)$ and $s_\phi(t)$, we obtain

$$\begin{aligned} \dot{s}_{vb} =& s_\phi, \\ \dot{s}_\phi =& \delta(t) + v(t), \end{aligned} \tag{35}$$

where $\delta(t)$ is the total disturbance caused by parameter uncertainties, i.e. the degradation of the PEMFC and the external disturbance. For example, if $\ddot{v}_b^*(t)$ is not compensated, we would have $\delta(t) = -C\ddot{v}_b^*(t)$.

For system (35), the standard twisting control algorithm given by [22]

$$v(t) = -K_1 sign(s_{vb}) - K_2 sign(s_\phi), \tag{36}$$

drives both s_{vb} and s_ϕ to zero in a finite time, i.e. it provides the convergence of the DC bus voltage to its reference value if the control gains are chosen as $K_1 = \Upsilon$ and $K_2 = 0.5\Upsilon$ where $\Upsilon > 2\delta_{max}$ with $|\delta(t)| \leq \delta_{max}$.

The proof of the above statement using strict Lyapunov functions can be founded in [23, 41]. On the other hand, one can follow [22] and ensure the convergence of the twisting algorithm using a geometrical proof.

It should be noted that the application of this controller requires the assumption that the information of the load current is available. This assumption is frequently used in such domain as we can see in [4, 42].

4.3. Outer voltage controller

The main objective of the outer voltage loop focuses on controlling the SCs voltage by controlling the current of fuel cell indirectly and thereupon the DC bus voltage. As shown in Fig.5, the fuel cell current will be indirectly regulated by the variation of the DC bus voltage so as to keep the SCs current at its desired operating value. Referring to equation (1), the relationship between $i_{fc}(t)$ and $v_b(t)$ is nonlinear. Thus, the outer voltage loop is considered to utilize a small-signal model approach, which means that near the operating point of fuel cell, the linearization is made for equation (1). Then, the variation relationship between $\delta i_{fc}(t)$ and $\delta v_b(t)$ can be presented as follows.

$$\delta i_{fc}(t) = -H\delta v_b(t), \tag{37}$$

where H is a positive parameter with the range of $[H_{\_min}, H_{\_max}]$.

The outer voltage controller is on the basis of PI controller, which is designed as follows.

$$v_b^* = k_p(v_{sc}^* - v_{sc}) + k_i \int (v_{sc}^* - v_{sc})dt, \tag{38}$$

where k_p is the gain of the proportional term and k_i is the gain of the integral term.

4.4. Limitation constraints

In order to ensure the security of fuel cell and SCs, some limitation constraints are taken into account in the proposed control strategy. These constraints are integrated as dynamic saturation functions for the inner and the outer voltage loops.

In this paper, the constraint of SCs current is a dynamic saturation process, which can be illustrated in Fig.6.

The security voltage range of SCs is presented in equation (39). Within this security range, the security thresholds of SCs reference voltage are defined as equation (40) so as to guarantee the safe operation of SCs in charge mode and in discharge mode.

$$v_{sc} \in [v_{sc\_min}, v_{sc\_max}] \tag{39}$$

$$v_{sc}^* \in [v_{sc\_low}, v_{sc\_high}] \tag{40}$$

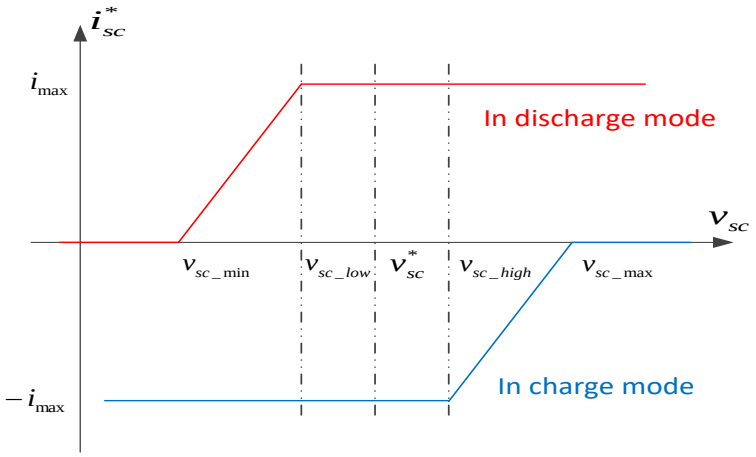

Figure 6: Limitation constraints of SCs current

In Fig.6, the red curve shows the SCs operates in discharge mode. If SCs voltage reaches v_{sc_low}, the absolute value of SCs reference current will decrease very soon until SCs voltage reaches v_{sc_min}. On the other hand, the blue curve shows the SCs operates in charge mode. When the SCs voltage reaches v_{sc_high}, the absolute value of SCs reference current will drop rapidly until SCs voltage reaches v_{sc_max}.

The limitations of SCs reference current mentioned above are presented as mathematical expressions equation (41) and (42). These two constraints are integrated in the saturation scheme of the inner voltage loop so as to avoid the occurrence of integral saturation.

$$i_{sc\_max\_cha} = i_{max} \cdot max\left(-1, min\left(0, \frac{v_{sc} - v_{sc\_max}}{v_{sc\_max} - v_{sc\_high}}\right)\right) \tag{41}$$

$$i_{sc\_max\_dis} = i_{max} \cdot min\left(1, max\left(0, \frac{v_{sc} - v_{sc\_min}}{v_{sc\_low} - v_{sc\_min}}\right)\right) \tag{42}$$

Moreover, the constraints of fuel cell current are integrated in the anti-windup scheme of the outer voltage loop in order to prevent the integral saturation. Due to the fact that the fuel cell is linked to the load directly, the current of fuel cell cannot be controlled directly. Therefore, the DC bus voltage is adjusted between the dynamic security thresholds $[v_{b\_min\_dyn}, v_{b\_max\_dyn}]$, so as to limit the fuel cell discharge current in the security range $[v_{b\_min}, v_{b\_max}]$, as shown in the following equations.

$$v_{b\_max\_dyn} = v_b^* + K_{ifc} i_{fc}(t), \tag{43}$$

$$v_{b\_min\_dyn} = v_b^* + K_{ifc}(i_{fc}(t) - i_{fc\_max\_dis}). \tag{44}$$

5. HIL test results

The proposed control strategy for the single converter hybrid fuel cell/SCs power system taking into consideration the PEMFC degradation is validated by a HIL test bench. This test bench consists of two dSPACE DS1104 real-time board cards as shown in Fig.7. One dSPACE is used as hardware controller to implement the proposed control strategy and to validate its feasibility in real time. On the other hand, the other one is utilized as emulator to emulate the single converter hybrid fuell cell/SCs power system. For the realization of the HIL test bench, we have used a sampling frequency of 10 kHz for both dSPACE cards [43]. The degradation rate estimated in section 3 is adopted in the HIL test system. For SCs, the initial reference voltage v_{scref} is set as 125V, v_{sc_min} and v_{sc_low} are set as $0.5v_{scref}$ and $0.75v_{scref}$ respectively, v_{sc_max} and v_{sc_high} are set as 136V and 131V respectively. For fuel cell, the discharge limitation current $i_{fc\_max\_dis}$ is set as 80A. For DC bus voltage, the security range is set as [26V,38V].

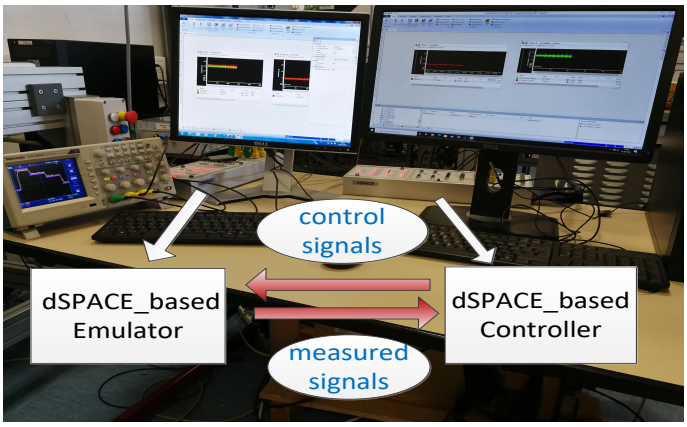

Figure 7: Scheme of HIL test system

In this section, the HIL test results are carried out by connecting the load affected by perturbations to the hybrid fuel cell/SCs power sources.

The load current curve adopted in this HIL test is a superposition of a step demand current curve and a sinusoidal perturbation current curve. The frequency and amplitude of the sinusoidal perturbation current are 7.5Hz and 3A respectively.

5.1. HIL test results of the proposed control strategy

The HIL test results of the proposed control strategy for hybrid fuel cell/SCs power system are shown in Fig.8 and Fig.9. According to these two figures, after utilizing the proposed control strategy, the perturbations on fuel cell current have been attenuated to a large extent due to the fact that SCs absorb the transient and sinusoidal perturbations effectively. The control strategy proposed in this paper can smooth the behavior of fuel cell current, which benefits to the lifespan of PEMFC.

Fig.8 presents the condition in nominal mode, in which all of the current and voltage values are in the allowed range. The dynamic DC bus voltage thresholds keep constant all the time, which means the saturation function is not activated. As shown in Fig.8(a),(c),(d), at the time of 10s and 140s, with the sudden increase of the load current, SCs operate as the auxiliary power source discharges rapidly and provide the current in transient process. Subsequently, the fuel cell with lower dynamic operates as the main power source. On the other hand, when the load current decreases suddenly at the time of 70s and 210s, the mode of SCs changes to the charge mode quickly. After that, fuel cell works as the main power source. Moreover, the value of SCs voltage is regulated at the desired security operating range and the convergence of DC bus voltage is validated for the proposed control method.

Fig.9 presents the condition when the fuel cell discharge current reaches the limitation threshold. In this condition, the saturation function is activated so as to protect the fuel cell. As shown in Fig.9(c), from 10s to 70s, the fuel cell current is limited at $i_{fc\_max\_dis}$, namely the value of 80A.

5.2. Comparison with HIL test results of two PI controllers method

In order to make further analysis of the proposed control strategy, the HIL tests of the same hybrid fuel cell/SCs power system with two PI controllers are implemented as well. In other words, the HIL tests are made after replacing the twisting controller with the integrator in inner voltage loop by a traditional PI controller and the outer voltage loop adopts PI controller still. Fig.10 presents the comparison HIL test results of fuel cell current between the traditional method on the basis of two PI controllers and the proposed

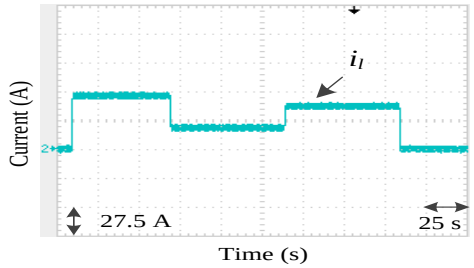

(a) Load current i_l

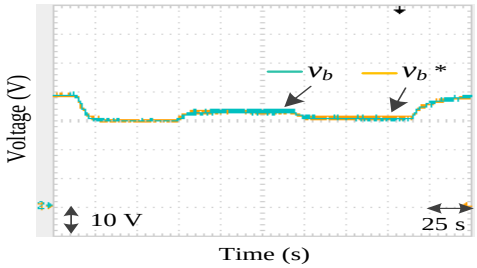

(b) Bus voltage v_b and reference v_b^*

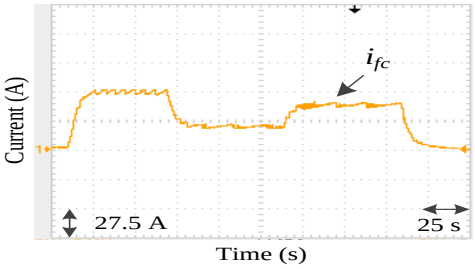

(c) Fuel cell current i_{fc}

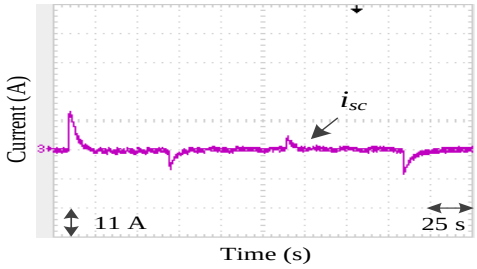

(d) Super capacitors current i_{sc}

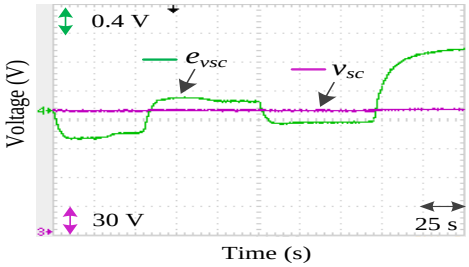

(e) Super capacitors voltage v_{sc} and error e_{vsc}

Figure 8: HIL test results in nominal mode

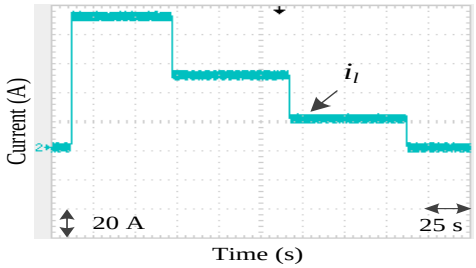

(a) Load current i_l

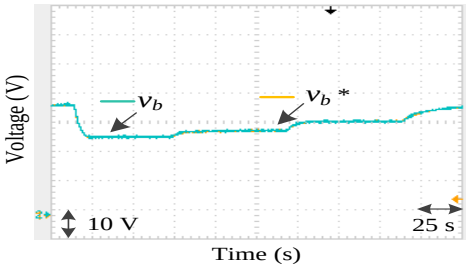

(b) Bus voltage v_b and reference v_b^*

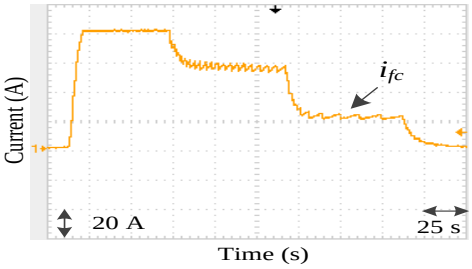

(c) Fuel cell current i_{fc}

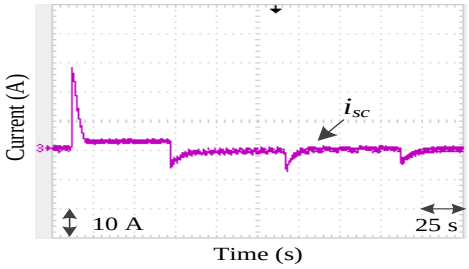

(d) Super capacitors current i_{sc}

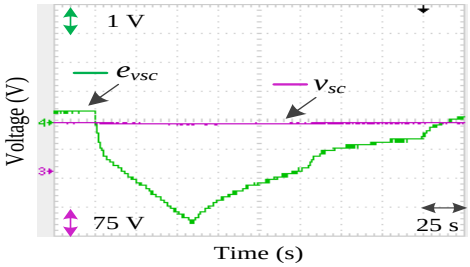

(e) Super capacitors voltage v_{sc} and error e_{vsc}

Figure 9: HIL test results in discharge limitation mode

control method which is based on one twisting controller used in inner voltage loop and one PI controller used in the outer loop. It can be seen that the oscillations of fuel cell current by the proposed method are smaller than two PI method. For proposed method, the oscillation amplitude of the sinusoidal oscillations on the fuel cell current is 0.165A; for two PI method, the oscillation amplitude of the sinusoidal oscillations on the fuel cell current is 0.86A. That is to say, the fuel cell current of the proposed method is smoother than the method of two PI controllers.

The change of fuel cell current will bring challenges to fuel cell water management, thermal management and gas management [44, 45]. Moreover, the changing fuel cell current will accelerate the degradation of the fuel cell membrane, catalyst and gas diffusion layer [45, 46]. For example, the changing current will cause the catalyst particles to become coarse and lead to the change of the oxide coverage degree of platinum and carbon, and the surface hydrophobicity [47, 48]. In addition, the durability comparison experiments show that the degradation rate of fuel cells under constant current is lower than that of fuel cells under dynamic current with oscillations [49]. Overall, the smoother fuel cell current results in the lower degradation rate, which is better for the lifespan of fuel cells. Hence, compared with two PI controllers method, our proposed method can increase the lifespan of fuel cell better.

Therefore, the proposed method in this paper based on the combination of twisting controller and PI controller is better than the control method based on two PI controllers in terms of perturbation suppression.

6. Conclusion

In this paper, considering the degradation of PEMFC, a novel second order sliding mode control strategy for hybrid fuel cell/super capacitors power system on the basis of only one converter has been presented. In this hybrid power system, fuel cell and super capacitors are performed as the main source and auxiliary source respectively. The degradation state and degradation rate of the PEMFC degradation model are estimated using the CKF method and are taken into account in the hybrid system. In this hybrid system, the proposed control strategy utilizes the twisting controller for the inner voltage loop and the proportional integral controller for the outer voltage loop. Moreover, some limitation constraints are taken into account so as to protect and increase the lifespan of the hybrid power sources. Finally, the effectiveness of the proposed control strategy is verified by HIL test bench.

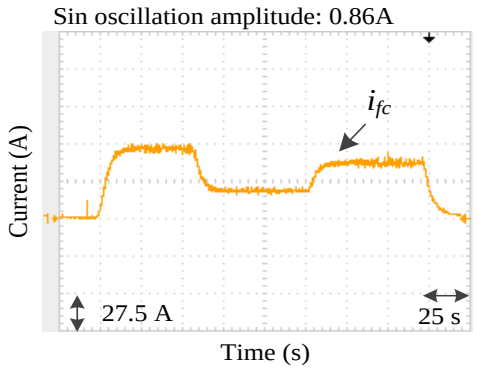

(a) 2PI - in nominal mode

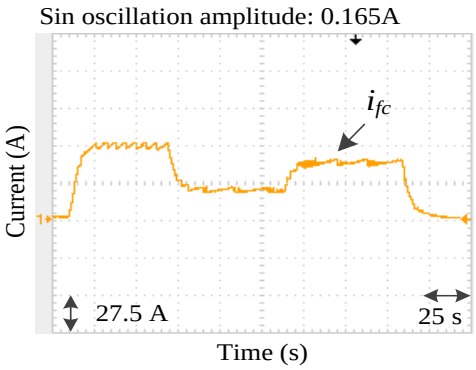

(b) Proposed method - in nominal mode

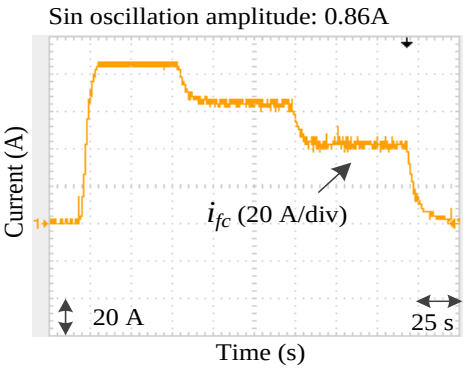

(c) 2PI - in discharge limitation mode

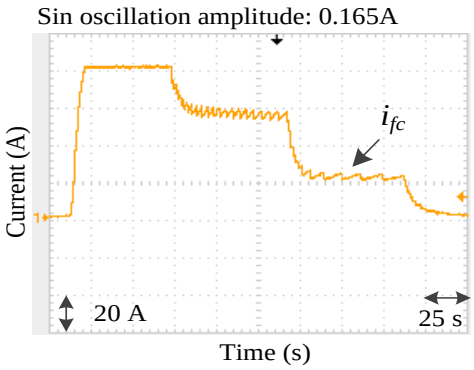

(d) Proposed method - in discharge limitation mode

Figure 10: Comparison of the proposed method and two PI controllers method - Fuel cell current i_{fc}

In future research work, there are two aspects which will be considered. Firstly, consider to design the adaptive version of the current algorithm in order to avoid overestimating the gains. Secondly, try to propose an algorithm that does not need the information of load current which is considered as an unknown perturbation.

References

[1] Toghyani, S., Afshari, E., Baniasadi, E.. Performance evaluation of an integrated proton exchange membrane fuel cell system with ejector absorption refrigeration cycle. Energy Conversion and Management 2019;185:666–677.

[2] Kolli, A., Gaillard, A., De Bernardinis, A., Bethoux, O., Hissel, D., Khatir, Z.. A review on dc/dc converter architectures for power fuel cell applications. Energy Conversion and Management 2015;105:716–730.

[3] Sorrentino, M., Cirillo, V., Nappi, L.. Development of flexible procedures for co-optimizing design and control of fuel cell hybrid vehicles. Energy Conversion and Management 2019;185:537–551.

[4] Hilairet, M., Bethoux, O., Ghanes, M., Tanasa, V., Barbot, J.P., Normand-Cyrot, M.D.. Experimental validation of a sampled-data passivity-based controller for coordination of converters in a fuel cell system. IEEE Transactions on Industrial Electronics 2014;62(8):5187–5194.

[5] Seyhan, M., Akansu, Y.E., Murat, M., Korkmaz, Y., Akansu, S.O.. Performance prediction of pem fuel cell with wavy serpentine flow channel by using artificial neural network. International Journal of Hydrogen Energy 2017;42(40):25619–25629.

[6] Budak, Y., Devrim, Y.. Investigation of micro-combined heat and power application of pem fuel cell systems. Energy Conversion and Management 2018;160:486–494.

[7] Authayanun, S., Hacker, V.. Energy and exergy analyses of a standalone ht-pemfc based trigeneration system for residential applications. Energy conversion and management 2018;160:230–242.

[8] Chen, K., Laghrouche, S., Djerdir, A.. Degradation model of proton exchange membrane fuel cell based on a novel hybrid method. Applied Energy 2019;252:113439.

[9] Hilairet, M., Bethoux, O., Azib, T., Talj, R.. Interconnection and damping assignment passivity-based control of a fuel cell system. In: 2010 IEEE International Symposium on Industrial Electronics. IEEE; 2010, p. 219–224.

[10] Tiefensee, F., Hilairet, M., Normand-Cyrot, D., Bethoux, O.. Sampled-data energetic management of a fuel cell/supercapacitor system. In: 2010 IEEE Vehicle Power and Propulsion Conference. IEEE; 2010, p. 1–6.

[11] Mane, S., Kazi, F., Singh, N.. Fuel cell and ultra-capacitor based hybrid energy control using ida-pbc methodology. In: 2015 International Conference on Industrial Instrumentation and Control (ICIC). IEEE; 2015, p. 879–884.

[12] Azib, T., Bethoux, O., Remy, G., Marchand, C.. Structure and control strategy for a parallel hybrid fuel cell/supercapacitors power source. In: 2009 IEEE Vehicle Power and Propulsion Conference. IEEE; 2009, p. 1858–1863.

[13] Talj, R., Ortega, R., Astolfi, A.. Passivity and robust pi control of the air supply system of a pem fuel cell model. Automatica 2011;47(12):2554–2561.

[14] Hilairet, M., Bethoux, O.. A passive controller-observer for coordination of converters in a fuel cell system. In: 2011 IEEE International Symposium on Industrial Electronics. IEEE; 2011, p. 2209–2214.

[15] Li, H., Ravey, A., NDiaye, A., Djerdir, A.. Online adaptive equivalent consumption minimization strategy for fuel cell hybrid electric vehicle considering power sources degradation. Energy Conversion and Management 2019;192:133–149.

[16] Li, H., Ravey, A., N'Diaye, A., Djerdir, A.. A novel equivalent consumption minimization strategy for hybrid electric vehicle powered by fuel cell, battery and supercapacitor. Journal of Power Sources 2018;395:262–270.

[17] Laghrouche, S., Plestan, F., Glumineau, A.. Higher order sliding mode control based on integral sliding mode. Automatica 2007;43(3):531–537.

[18] Sanchez, T., Moreno, J.A., Fridman, L.M.. Output feedback continuous twisting algorithm. Automatica 2018;96:298–305.

[19] Han, T., Hu, Q.. Robust autopilot design for STT missiles with multiple disturbances using twisting control. Aerospace Science and Technology 2017;70:428–434.

[20] Boiko, I.M.. On frequency-domain criterion of finite-time convergence of second-order sliding mode control algorithms. Automatica 2011;47(9):1969–1973.

[21] Shtessel, Y.B., Shkolnikov, I.A., Levant, A.. Smooth second-order sliding modes: Missile guidance application. Automatica 2007;43(8):1470–1476.

[22] Levant, A.. Sliding order and sliding accuracy in sliding mode control. International journal of control 1993;58(6):1247–1263.

[23] Sánchez, T., Moreno, J.A.. Lyapunov functions for twisting and terminal controllers. In: 2014 13th International Workshop on Variable Structure Systems (VSS). IEEE; 2014, p. 1–6.

[24] Kamal, S., Moreno, J.A., Chalanga, A., Bandyopadhyay, B., Fridman, L.M.. Continuous terminal sliding-mode controller. Automatica 2016;69:308–314.

[25] Chen, K., Laghrouche, S., Djerdir, A.. Degradation prediction of proton exchange membrane fuel cell based on grey neural network model and particle swarm optimization. Energy Conversion and Management 2019;195:810–818.

[26] Jouin, M., Gouriveau, R., Hissel, D., Péra, M.C., Zerhouni, N.. Joint particle filters prognostics for proton exchange membrane fuel cell power prediction at constant current solicitation. IEEE Transactions on reliability 2015;65(1):336–349.

[27] Gouriveau, R., Hilairet, M., Hissel, D., Jemei, S., Jouin, M., Lechartier, E., et al. IEEE PHM 2014 data challenge: Outline, experiments, scoring of results, winners. IEEE 2014 PHM Challenge, Tech Rep 2014;.

[28] Larminie, J., Dicks, A., McDonald, M.S.. Fuel cell systems explained; vol. 2. J. Wiley Chichester, UK; 2003.

[29] Wahdame, B., Candusso, D., François, X., Harel, F., Péra, M.C., Hissel, D., et al. Comparison between two pem fuel cell durability tests performed at constant current and under solicitations linked to transport mission profile. International Journal of Hydrogen Energy 2007;32(17):4523–4536.

[30] Wei, L., Wu, M., Yan, M., Liu, S., Cao, Q., Wang, H.. A review on electrothermal modeling of supercapacitors for energy storage applications. IEEE Journal of Emerging and Selected Topics in Power Electronics 2019;7(3):1677–1690.

[31] Bressel, M., Hilairet, M., Hissel, D., Bouamama, B.O.. Remaining useful life prediction and uncertainty quantification of proton exchange membrane fuel cell under variable load. IEEE Transactions on Industrial Electronics 2016;63(4):2569–2577.

[32] Bressel, M., Hilairet, M., Hissel, D., Bouamama, B.O.. Extended kalman filter for prognostic of proton exchange membrane fuel cell. Applied Energy 2016;164:220–227.

[33] Liu, H., Chen, J., Hissel, D., Su, H.. Remaining useful life estimation for proton exchange membrane fuel cells using a hybrid method. Applied energy 2019;237:910–919.

[34] Arasaratnam, I., Haykin, S.. Cubature kalman filters. IEEE Transactions on automatic control 2009;54(6):1254–1269.

[35] Haykin, S., Arasaratnam, I.. Cubature kalman filters. IEEE Trans Autom Control 2009;54(6):1254–1269.

[36] Cui, B., Wei, X., Chen, X., Li, J., Li, L.. On sigma-point update of cubature kalman filter for gnss/ins under gnss-challenged environment. IEEE Transactions on Vehicular Technology 2019;68(9):8671–8682.

[37] Torres-González, V., Sanchez, T., Fridman, L.M., Moreno, J.A.. Design of continuous twisting algorithm. Automatica 2017;80:119–126.

[38] Rakhtala, S.M., Ahmadi, M.. Twisting control algorithm for the yaw and pitch tracking of a twin rotor uav. International Journal of Automation and Control 2017;11(2):143–163.

[39] Zhang, L., Zhang, H., Obeid, H., Laghrouche, S.. Time-varying state observer based twisting control of linear induction motor considering dynamic end effects with unknown load torque. ISA transactions 2019;93:290–301.

[40] Fridman, L., Moreno, J.A., Bandyopadhyay, B., Kamal, S., Chalanga, A.. Continuous nested algorithms: The fifth generation of sliding mode controllers. In: Recent advances in sliding modes: From control to intelligent mechatronics. Springer; 2015, p. 5–35.

[41] Santiesteban, R., Fridman, L., Moreno, J.A.. Finite-time convergence analysis for twisting controller via a strict lyapunov function. In: 2010 11th international workshop on variable structure systems (VSS). IEEE; 2010, p. 1–6.

[42] Hilairet, M., Ghanes, M., Béthoux, O., Tanasa, V., Barbot, J.P., Normand-Cyrot, D.. A passivity-based controller for coordination of converters in a fuel cell system. Control engineering practice 2013;21(8):1097–1109.

[43] Zhang, Y., Xiong, R., He, H., Shen, W.. Lithium-Ion Battery Pack State of Charge and State of Energy Estimation Algorithms Using a Hardware-in-the-Loop Validation. IEEE Transactions on Power Electronics 2017;32(6):4421–4431.

[44] Chen, H., Zhao, X., Qu, B., Zhang, T., Pei, P., Li, C.. An evaluation method of gas distribution quality in dynamic process of proton exchange membrane fuel cell. Applied Energy 2018;232:26–35.

[45] Ren, P., Pei, P., Li, Y., Wu, Z., Chen, D., Huang, S.. Degradation mechanisms of proton exchange membrane fuel cell under typical automotive operating conditions. Progress in Energy and Combustion Science 2020;80:100859.

[46] Borup, R.L., Davey, J.R., Garzon, F.H., Wood, D.L., Inbody, M.A.. Pem fuel cell electrocatalyst durability measurements. Journal of Power Sources 2006;163(1):76–81.

[47] Heyd, D.V., Harrington, D.A.. Platinum oxide growth kinetics for cyclic voltammetry. Journal of Electroanalytical Chemistry 1992;335(1-2):19–31.

[48] Borup, R., Meyers, J., Pivovar, B., Kim, Y.S., Mukundan, R., Garland, N., et al. Scientific aspects of polymer electrolyte fuel cell durability and degradation. Chemical reviews 2007;107(10):3904–3951.

[49] Ibrahim, M., Steiner, N.Y., Jemei, S., Hissel, D.. Wavelet-based approach for online fuel cell remaining useful lifetime prediction. IEEE Transactions on Industrial Electronics 2016;63(8):5057–5068.